

# Appendix 1

## Methodology and data cross-plots

### *Gamma-ray spectrometry*

Outcrops appearing on Figure 3 of the main text and on Cross-sections A-A' and B-B' (Fig. A1-1, Appendix 3) were surveyed in the field with the RS-230 BGO scintillometer of Radiation Solutions Inc. (Kabanov et al., 2016a, 2016c). SGR logs were made mostly at 0.5 m step in mudrock-dominated sections and with 1.0 m step in carbonate sections. Measurements across stratigraphic contacts associated with significant lithological change were made with more frequent increments. Signal acquisition time was set to 90 seconds. Wells drilled in 2012-2014 in the central Mackenzie Valley by MDM Energy, Shell, Conoco Phillips, and Husky Energy (Cross-section A-A') were logged with Baker Hughes Digital Spectralog setup (Husky, MGM) and Schlumberger HNGS tool (Conoco Phillips). Well files of oil and gas N.W.T. and Yukon exploration wells are archived at NEB Core & Sample Repository of GSC Calgary. PDF versions of recently drilled wells are available through request to the NEB Frontier Office in Calgary (<https://www.neb-one.gc.ca/cntcts/index-eng.html>).

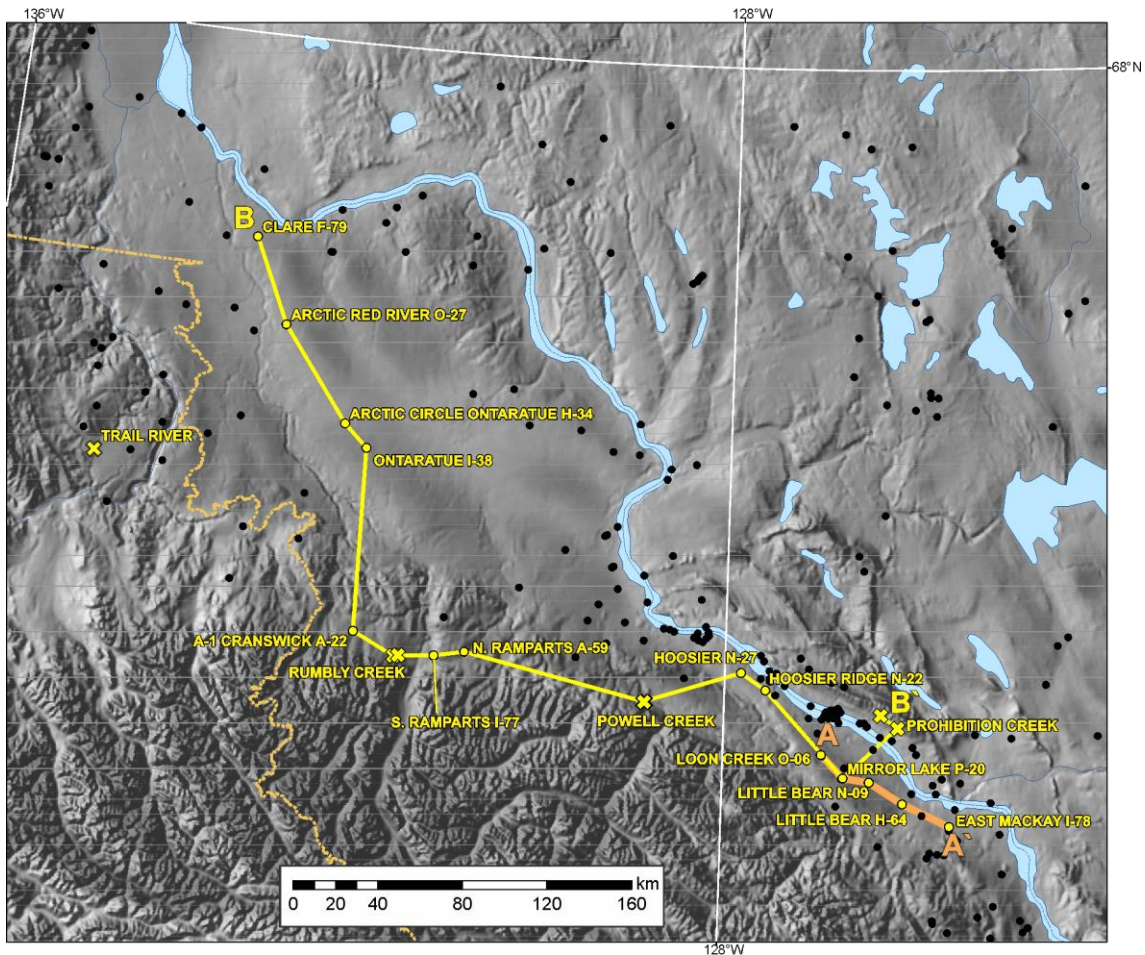


Figure A1-1. Traces of cross-sections A-A' and B-B'. Outcrops are marked with crosses, wells with circles (yellow if placed on cross-sections).

Decomposition of gamma radiation into U, Th and K spectra is widely used to interpret lithology and depositional environments. Potassium and thorium are relatively stable and mostly bound in detrital siliciclastics, whereas uranium is more soluble and tends to be trapped by organic matter. Hence, K and Th are usually better correlated to each other than K/U and Th/U and are often used together as K-Th gamma ray proxy for siliciclastic supply, also known as the computed gamma ray (CGR). Potassium is more involved in weathering mineral transformations than thorium and therefore tends to be bound in clays. Thorium is relatively stable near the Earth surface and preferentially resides in detrital grains. The contribution of K, U, and Th series to the total GR is approximated by the formula (Ellis and Singer, 2008):

$$\text{GR[API]} = 4 \times \text{Th[ppm]} + 8 \times \text{U[ppm]} + 16 \times \text{K [wt.\%]}$$

The gamma-ray spectrometry is based on the fact that natural radioactivity in pre-Cenozoic rocks mostly results from three isotopes,  $^{232}\text{Th}$ ,  $^{40}\text{K}$ , and  $^{238}\text{U}$ , having half-lives comparable to the age of the Earth crust. Other radioactive isotopes decay faster with diminutive significance back in the pre-Quaternary geological record. Thorium and uranium both decay through two different series of a dozen or more intermediate isotopes to a stable isotope of lead. These decays produce complicated gamma-ray spectra with energy emission lines characteristic for each series. Radioactive potassium  $^{40}\text{K}$  decaying to stable  $^{39}\text{K}$  has only one characteristic gamma energy of 1.46 MeV (Myers and Wignall, 1987; Ellis and Singer, 2008).

Use of potassium from SGR spectrometry as a proxy to alumina content is based on strong linear covariation of Al and K observed from 1687 ICP elemental data as measured by Pearson  $r = 0.95$  and origin-forced linear regression  $R^2 = 0.93$  (Fig. A1-2). These data include Hare Indian, Canol, and basal Imperial subsets. Data from the upper Ramparts and Hume limestones are excluded for being dominantly lean in siliciclastics and producing anomalous values the same way as Al-normalized trace metals (Tribovillard et al., 2006). Similarly to U/Al proxy to the authigenic enrichment of U, normalized uranium ( $U_n$ ) is calculated from SGR as follows:

$$U_n = 0.29 \times \text{U[ppm]} / \text{K[wt.\%]}$$

The slope of 0.29 in this equation scales  $U_n$  down to U/Al.

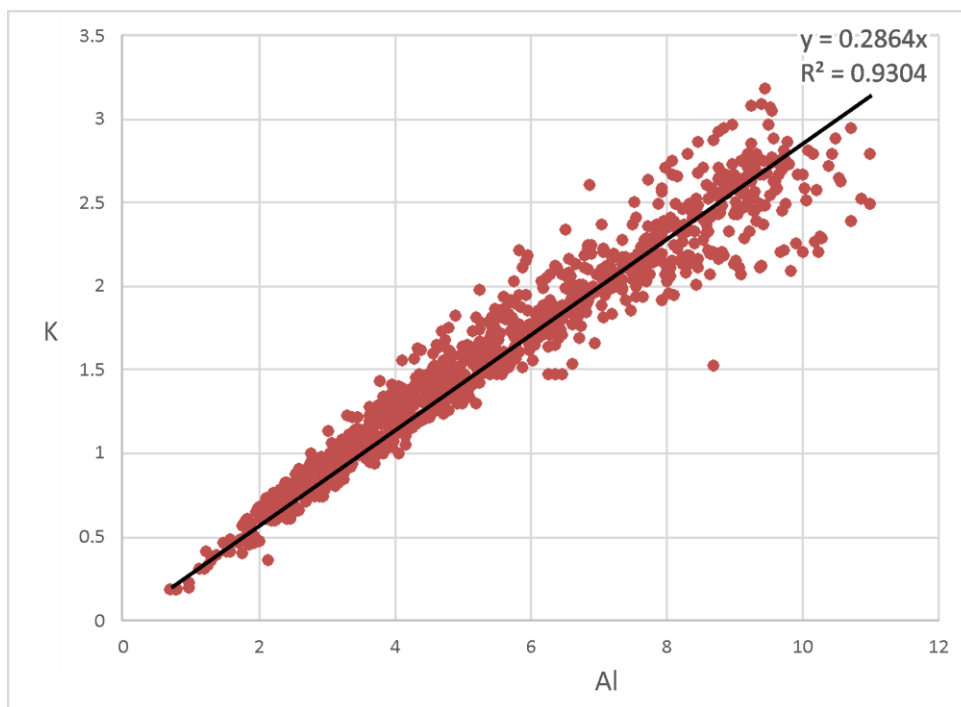


**Figure A1-2. Al/K cross-plot for mudrocks of the Horn River Group and basal Imperial Formation, ICP elemental data in wt.% (Appendix 4).**

### *ICP elemental geochemistry*

The samples were analyzed for elemental concentration at Bureau Veritas (former Acme) Analytical Laboratories in Vancouver, BC using the inductively coupled plasma-mass spectrometry (ICP-MS, ICP-ES) instrumentation technique and two main protocols of sample preparation. The litho-geochemical whole rock fusion protocol was similar for all sample batches (Acme/BV analytical code 4A) reported in Appendix 4. This involves mixing a 200 mg sample with a lithium metaborate ( $\text{LiBO}_2$ )/ lithium tetraborate ( $\text{Li}_2\text{B}_4\text{O}_7$ ) flux in a crucible. The crucibles are then placed in a furnace and heated in order to fuse the sample. The bead that develops is cooled then dissolved in nitric acid and run for ICP-MS in order to analyze the concentrations of rare earth and refractory elements (11 compounds, 33 elements). LOI is also measured by heating to  $1000^\circ\text{C}$  and then weighing an aliquot of the sample in order to determine weight loss. This is used as a rough approximation of organic matter (carbon) minus water and light hydrocarbons that were burned off.

The second technique was aqua regia digestion (Acme/BV codes AQ200, 1DX) whereby 500 mg of sample was digested in a 1:1:1 solution of hydrochloric acid (HCl), nitric acid ( $\text{HNO}_3$ ) and de-ionized water while placed in a heated water bath for one hour. Dilute HCl was then added to the residue in order to top up the sample to the required analysis volume. Samples were split into 0.5g subsamples and run through the ICP-MS instrument to determine the concentration of 14 elements that were not detected in the above technique, including Au and volatile elements, at the ppm level. The AQ200/1DX has been ordered for most sample batches (Pyle et al., 2011; Pyle and Gal, 2012; Gal and Pyle, 2012; Pyle and Gal, 2013; Kabanov et al., 2015; Kabanov et al., 2016a; Hutchison and Fraser, 2015; Fraser and Hutchison, 2017). Geochemical, XRD, and thermal maturity data from the NTGS Mackenzie Valley Petroleum Project first appeared in a number of open reports (Pyle et al., 2011; Pyle and Gal, 2012; Gal

and Pyle, 2012; Pyle and Gal, 2013) and subsequently were bundled together in concluding volume (Pyle et al., 2014). GSC geochemical data compiled in Appendix 3 were reported by Kabanov (2015, 2017), Kabanov et al. (2015, 2016a) and the Trail River data published by Hutchison and Fraser (2015) and Fraser and Hutchison (2017).

The AQ200 is substituted with the 4-acid digestion (BV's code MA200) in the batch reported by Kabanov (2017). This allows for more complete release of chalcophile elements than in the previously used aqua regia solution (AQ200). A 0.25 g split is heated in HNO<sub>3</sub>-HClO<sub>4</sub>-HF to fuming and taken to dryness. The residue is dissolved in HCl, made to volume with dilute HCl, and analyzed by the ICP-ES/MS.

In addition, total carbon and total sulphur were measured using the LECO instrument. In this procedure, the induction flux is added to the crushed sample and ignited in an induction furnace. A carrier gas sweeps up the released carbon which is measured by adsorption in an infrared spectrometric cell. The results represent all forms of carbon and sulphur that are present in the sample. The detection limit for this procedure is 0.02%.

Linear correlation matrices of geochemical proxies that are discussed in the main text are given on Tables A1-1 through A1-6, and cross-plots of these proxies are given on Figures A1-3 through A1-9. The data on scatterplots are smoothed with LOWESS regression, which stands for *locally weighted scatterplot smoother* (Cleveland, 1979). LOWESS (= LOESS for multivariate data) is a robust non-parametric least-squares polynomial method. The  $\alpha$ -tension is parameter ranging from 0 to 1 which determines the width of the sliding window, i.e. proportion of observations used in each local regression; decrease of  $\alpha$ -tension moves the smoother towards single data points. Computation procedure cannot be described by one formula and is given elsewhere (Cleveland and Devlin, 1988; Jacoby, 2000).

	TOC	P	EFP	Al	K	Fe	TIP	SiO <sub>2</sub>	SiO <sub>2</sub> /Zr	EFMo	EFU	EFcd	EFZn	EFcu	EFBa	DOPt	Mo/TOC	TOC/P
TOC	1.0																	
P	0.1	1.0																
EFP	0.1	0.5	1.0															
Al	-0.3	0.2	-0.5	1.0														
K	-0.2	0.3	-0.5	1.0	1.0													
Fe	-0.1	0.3	-0.2	0.5	0.5	1.0												
TIP	-0.2	0.3	-0.5	1.0	1.0	0.5	1.0											
SiO <sub>2</sub>	0.1	-0.3	-0.2	-0.3	-0.3	-0.5	-0.3	1.0										
SiO <sub>2</sub> /Zr	0.0	-0.4	0.2	-0.7	-0.7	-0.5	-0.7	0.6	1.0									
EFMo	0.4	-0.1	0.2	-0.6	-0.6	-0.3	-0.6	0.5	0.6	1.0								
EFU	0.4	0.0	0.4	-0.6	-0.6	-0.2	-0.6	0.3	0.5	0.8	1.0							
EFcd	0.2	0.2	0.3	-0.3	-0.3	0.0	-0.3	0.0	0.1	0.3	0.4	1.0						
EFZn	0.1	0.1	0.3	-0.3	-0.4	0.0	-0.3	0.2	0.3	0.6	0.6	0.7	1.0					
EFcu	0.3	0.2	0.3	-0.4	-0.4	0.1	-0.4	0.1	0.2	0.6	0.6	0.6	0.6	1.0				
EFBa	-0.1	0.0	0.3	-0.2	-0.2	-0.1	-0.2	-0.2	0.1	0.0	0.1	0.0	0.0	0.0	1.0			
DOPt	0.3	-0.1	0.1	-0.3	-0.3	-0.1	-0.3	0.1	0.2	0.3	0.3	0.1	0.2	0.3	0.0	1.0		
Mo/TOC	0.0	-0.1	-0.1	0.0	-0.1	0.1	0.0	0.2	0.1	0.6	0.3	0.2	0.4	0.3	-0.1	0.1	1.0	
TOC/P	0.5	-0.6	-0.3	-0.3	-0.3	-0.3	-0.4	0.3	0.4	0.3	0.2	-0.1	-0.1	0.0	-0.1	0.1	-0.1	1.0

**Table A1-1.** Pearson  $r$  linear correlation matrix of elemental proxies and TOC for Canol Formation (n=847), excluding the Trail River subset. Here and in Tables A1-2 through A1-6 significant covariance is marked green if >0.5 and grey if <-0.5.

	TOC	EFP	P	Al	K	Fe	TIP	SiO <sub>2</sub>	SiO <sub>2</sub> /Zr	EFMo	EFU	EFCd	EFZn	EFCu	EFBa	DOPt	Mo/TOC	TOC/P
TOC	1.00																	
EFP	0.01	1.00																
P	0.04	0.91	1.00															
Al	0.06	-0.40	-0.09	1.00														
K	0.08	-0.40	-0.10	0.98	1.00													
Fe	0.01	-0.12	-0.01	0.40	0.39	1.00												
TIP	0.07	-0.40	-0.09	1.00	0.99	0.41	1.00											
SiO <sub>2</sub>	-0.32	0.16	-0.09	-0.78	-0.76	-0.65	-0.78	1.00										
SiO <sub>2</sub> /Zr	-0.35	0.27	-0.02	-0.84	-0.85	-0.45	-0.85	0.81	1.00									
EFMo	0.05	0.19	-0.03	-0.55	-0.50	-0.21	-0.54	0.45	0.52	1.00								
EFU	0.26	0.32	0.13	-0.49	-0.46	-0.10	-0.49	0.20	0.32	0.76	1.00							
EFCd	-0.02	-0.01	0.02	0.04	0.02	0.14	0.03	-0.31	-0.04	0.10	0.22	1.00						
EFZn	-0.02	0.04	0.07	0.02	0.00	0.34	0.01	-0.38	-0.05	0.15	0.34	0.83	1.00					
EFCu	-0.03	0.05	0.01	-0.11	-0.11	0.43	-0.11	-0.09	0.08	0.20	0.16	0.06	0.25	1.00				
EFBa	0.25	0.21	0.08	-0.41	-0.43	0.02	-0.41	0.06	0.19	-0.04	0.27	-0.03	-0.06	0.02	1.00			
DOPt	0.51	-0.05	0.03	0.19	0.21	0.10	0.20	-0.25	-0.42	-0.35	-0.17	-0.18	-0.19	-0.15	0.30	1.00		
Mo/TOC	-0.21	-0.04	-0.13	-0.14	-0.10	-0.02	-0.14	0.21	0.27	0.83	0.57	0.17	0.21	0.19	-0.30	-0.46	1.00	
TOC/P	0.38	-0.59	-0.59	0.18	0.23	-0.02	0.19	-0.12	-0.22	-0.04	-0.08	-0.04	-0.10	-0.12	-0.05	0.35	-0.02	1.00

**Table A1-2.** Pearson *r* linear correlation matrix of elemental proxies and TOC for the Canol Formation at Trail River (n=116).

	TOC	P	EFP	Al	K	Fe	TIP	SiO <sub>2</sub>	SiO <sub>2</sub> /Zr	EFMo	EFU	EFCd	EFZn	EFCu	EFBa	DOPt	Mo/TOC	TOC/P
TOC	1.00																	
P	0.03	1.00																
EFP	-0.09	0.67	1.00															
Al	0.13	0.42	-0.32	1.00														
K	0.26	0.38	-0.33	0.96	1.00													
Fe	-0.04	0.64	0.03	0.78	0.70	1.00												
TIP	0.14	0.43	-0.31	1.00	0.97	0.78	1.00											
SiO <sub>2</sub>	0.41	0.37	-0.23	0.78	0.85	0.54	0.80	1.00										
SiO <sub>2</sub> /Zr	0.60	-0.09	-0.28	0.28	0.40	0.00	0.28	0.59	1.00									
EFMo	0.78	-0.13	-0.12	0.00	0.13	-0.17	0.01	0.34	0.76	1.00								
EFU	0.68	-0.06	0.12	-0.23	-0.13	-0.30	-0.23	0.18	0.55	0.86	1.00							
EFCd	0.58	-0.06	0.03	-0.07	0.00	-0.20	-0.08	0.27	0.60	0.77	0.91	1.00						
EFZn	0.63	-0.01	-0.04	0.05	0.13	-0.02	0.06	0.34	0.57	0.81	0.78	0.83	1.00					
EFCu	0.70	0.27	0.30	-0.04	0.08	0.01	-0.02	0.34	0.54	0.77	0.82	0.71	0.76	1.00				
EFBa	0.50	-0.14	-0.23	0.07	0.18	-0.02	0.08	0.36	0.77	0.61	0.37	0.31	0.36	0.43	1.00			
DOPt	0.53	-0.17	-0.26	0.21	0.36	-0.08	0.22	0.39	0.74	0.71	0.52	0.56	0.57	0.52	0.54	1.00		
Mo/TOC	0.33	-0.14	-0.37	0.37	0.43	0.11	0.36	0.41	0.67	0.63	0.30	0.35	0.45	0.30	0.53	0.70	1.00	
TOC/P	0.89	-0.30	-0.37	0.04	0.17	-0.23	0.04	0.30	0.60	0.73	0.59	0.51	0.55	0.48	0.49	0.56	0.41	1.00

**Table A1-3.** Pearson *r* linear correlation matrix of elemental proxies and TOC for the upper Hare Indian Formation excluding the Prohibition Creek Member (n=119).

	TOC	P	EFP	Al	K	Fe	TIP	SiO <sub>2</sub>	SiO <sub>2</sub> /Zr	EFMo	EFU	EFCd	EFZn	EFCu	EFBa	DOPt	Mo/TOC	TOC/P
TOC	1.00																	
P	0.47	1.00																
EFP	0.58	0.66	1.00															
Al	-0.41	0.02	-0.66	1.00														
K	-0.32	0.10	-0.60	0.98	1.00													
Fe	-0.51	0.11	-0.48	0.79	0.76	1.00												
TIP	-0.38	0.05	-0.65	1.00	0.99	0.79	1.00											
SiO <sub>2</sub>	0.55	-0.05	0.22	-0.40	-0.39	-0.74	-0.39	1.00										
SiO <sub>2</sub> /Zr	0.32	-0.20	0.47	-0.75	-0.78	-0.78	-0.77	0.62	1.00									
EFMo	0.77	0.41	0.56	-0.39	-0.32	-0.41	-0.37	0.33	0.34	1.00								
EFU	0.82	0.47	0.70	-0.53	-0.46	-0.48	-0.51	0.37	0.40	0.87	1.00							
EFCd	0.68	0.29	0.44	-0.37	-0.25	-0.42	-0.34	0.33	0.15	0.57	0.51	1.00						
EFZn	0.64	0.22	0.37	-0.35	-0.26	-0.42	-0.33	0.35	0.22	0.63	0.52	0.95	1.00					
EFCu	0.81	0.38	0.57	-0.50	-0.37	-0.47	-0.46	0.44	0.25	0.68	0.69	0.84	0.78	1.00				
EFBa	0.06	-0.03	0.23	-0.38	-0.38	-0.24	-0.39	0.10	0.32	-0.11	0.06	0.02	-0.03	0.08	1.00			
DOPt	0.66	-0.02	0.31	-0.43	-0.33	-0.73	-0.41	0.71	0.49	0.52	0.52	0.59	0.59	0.65	0.15	1.00		
Mo/TOC	-0.12	0.15	-0.35	0.65	0.66	0.51	0.66	-0.32	-0.51	0.28	-0.01	-0.08	0.02	-0.15	-0.52	-0.16	1.00	
TOC/P	0.21	-0.69	-0.27	-0.35	-0.37	-0.54	-0.35	0.55	0.46	0.06	0.07	0.16	0.20	0.18	0.05	0.50	-0.33	1.00

**Table A1-4.** Pearson *r* linear correlation matrix of elemental proxies and TOC for the Prohibition Creek Member (n=94).

	TOC	P	EFP	Al	K	Fe	TIP	SiO <sub>2</sub>	SiO <sub>2</sub> /Zr	EFMo	EFU	EFCd	EFZn	EFCu	EFBa	DOPt	Mo/TOC	TOC/P	
TOC	1.00																		
P	0.30	1.00																	
EFP	0.24	0.65	1.00							<b>BLUEFISH MEMBER</b>									
Al	-0.37	-0.13	-0.69	1.00															
K	-0.29	-0.14	-0.68	0.95	1.00														
Fe	-0.27	-0.05	-0.40	0.55	0.48	1.00													
TIP	-0.35	-0.13	-0.69	1.00	0.96	0.54	1.00												
SiO <sub>2</sub>	0.30	0.14	-0.16	0.11	0.17	-0.25	0.13	1.00											
SiO <sub>2</sub> /Zr	0.06	-0.11	0.30	-0.50	-0.52	-0.50	-0.51	0.41	1.00										
EFMo	0.54	0.27	0.50	-0.60	-0.55	-0.36	-0.59	0.22	0.41	1.00									
EFU	0.46	0.26	0.67	-0.66	-0.64	-0.37	-0.66	-0.14	0.35	0.78	1.00								
EFCd	0.43	0.25	0.57	-0.57	-0.52	-0.43	-0.57	0.09	0.17	0.37	0.43	1.00							
EFZn	0.28	0.49	0.70	-0.43	-0.43	-0.19	-0.43	-0.03	0.18	0.50	0.53	0.49	1.00						
EFCu	0.55	0.48	0.75	-0.72	-0.66	-0.43	-0.71	0.13	0.22	0.64	0.61	0.73	0.70	1.00					
EFBa	0.14	-0.12	0.15	-0.36	-0.41	-0.20	-0.36	-0.04	0.36	0.36	0.29	-0.03	0.07	0.17	1.00				
DOPt	0.31	-0.03	0.23	-0.41	-0.36	-0.32	-0.40	0.20	0.45	0.52	0.40	0.30	0.28	0.41	0.39	1.00			
Mo/TOC	-0.18	-0.02	-0.04	0.06	0.09	0.04	0.07	0.17	0.16	0.51	0.21	-0.22	0.13	-0.01	0.14	0.25	1.00		
TOC/P	0.49	-0.55	-0.30	-0.15	-0.06	-0.10	-0.14	0.06	0.07	0.15	0.12	0.14	-0.05	0.08	0.10	0.22	-0.18	1.00	

**Table A1-5.** Pearson *r* linear correlation matrix of elemental proxies and TOC for the Bluefish Member (n=173).

	TOC	P	EFP	Al	K	Fe	TIP	SiO <sub>2</sub>	SiO <sub>2</sub> /Zr	EFMo	EFU	EFCd	EFZn	EFCu	EFBa	DOPt	Mo/TOC	TOC/P	
TOC	1.00																		
P	0.06	1.00																	
EFP	0.36	0.81	1.00							<b>BASAL IMPERIAL FORMATION</b>									
Al	-0.60	-0.34	-0.77	1.00															
K	-0.47	-0.40	-0.79	0.94	1.00														
Fe	-0.60	0.05	-0.13	0.34	0.26	1.00													
TIP	-0.60	-0.33	-0.77	1.00	0.95	0.34	1.00												
SiO <sub>2</sub>	0.57	0.26	0.37	-0.50	-0.44	-0.76	-0.49	1.00											
SiO <sub>2</sub> /Zr	0.64	-0.24	0.13	-0.47	-0.41	-0.62	-0.49	0.52	1.00										
EFMo	0.82	0.07	0.46	-0.70	-0.56	-0.50	-0.70	0.55	0.67	1.00									
EFU	0.80	0.17	0.59	-0.77	-0.67	-0.43	-0.78	0.49	0.59	0.90	1.00								
EFCd	0.48	0.34	0.59	-0.70	-0.60	-0.30	-0.69	0.49	0.19	0.58	0.59	1.00							
EFZn	0.51	0.28	0.51	-0.61	-0.48	-0.38	-0.60	0.51	0.31	0.64	0.57	0.83	1.00						
EFCu	0.55	0.42	0.68	-0.77	-0.68	-0.23	-0.76	0.50	0.24	0.67	0.72	0.87	0.67	1.00					
EFBa	0.21	-0.01	0.21	-0.23	-0.27	0.00	-0.24	-0.02	0.31	0.25	0.33	-0.04	0.01	-0.02	1.00				
DOPt	0.73	-0.02	0.24	-0.51	-0.35	-0.63	-0.50	0.66	0.59	0.74	0.63	0.54	0.59	0.55	0.03	1.00			
Mo/TOC	0.25	-0.15	-0.03	-0.13	0.02	-0.16	-0.13	0.15	0.30	0.58	0.35	0.20	0.32	0.25	0.03	0.47	1.00		
TOC/P	0.76	-0.52	-0.20	-0.26	-0.15	-0.50	-0.27	0.29	0.65	0.57	0.49	0.11	0.16	0.14	0.17	0.55	0.25	1.00	

**Table A1-6.** Pearson *r* linear correlation matrix of elemental proxies and TOC for the Mirror Lake and Loon Creek members and unassigned basal shales of the Imperial Formation (n=282). Imperial Formation subset of Trail River is excluded.

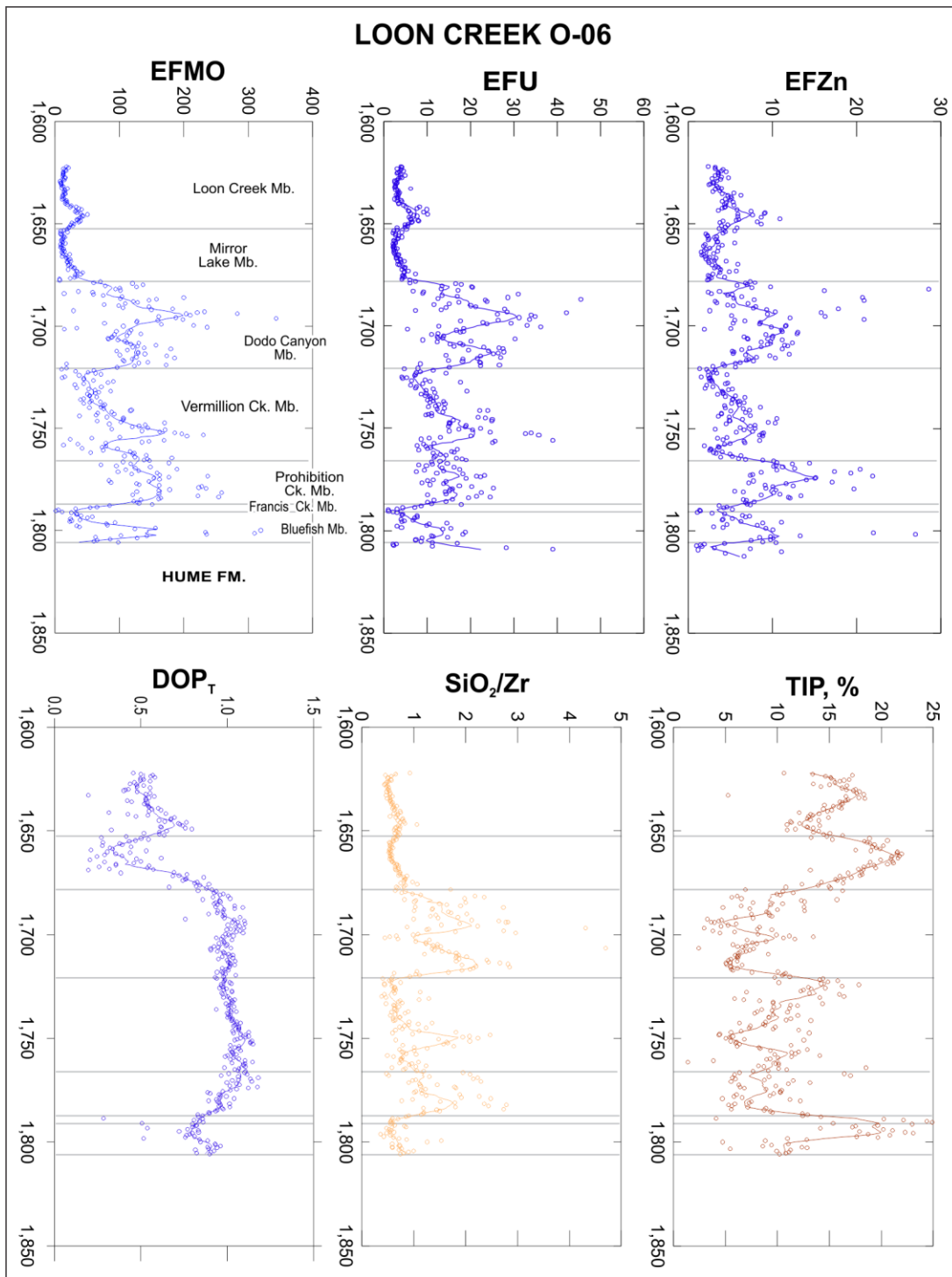


**Figure A1-3.** Loon Creek O-06. Supplementary scatterplots to Fig. 3 of the main text and log of EFZn. Solid lines are LOWESS regression with  $\alpha$ -tension 4%. Y axis is measured depth, m.

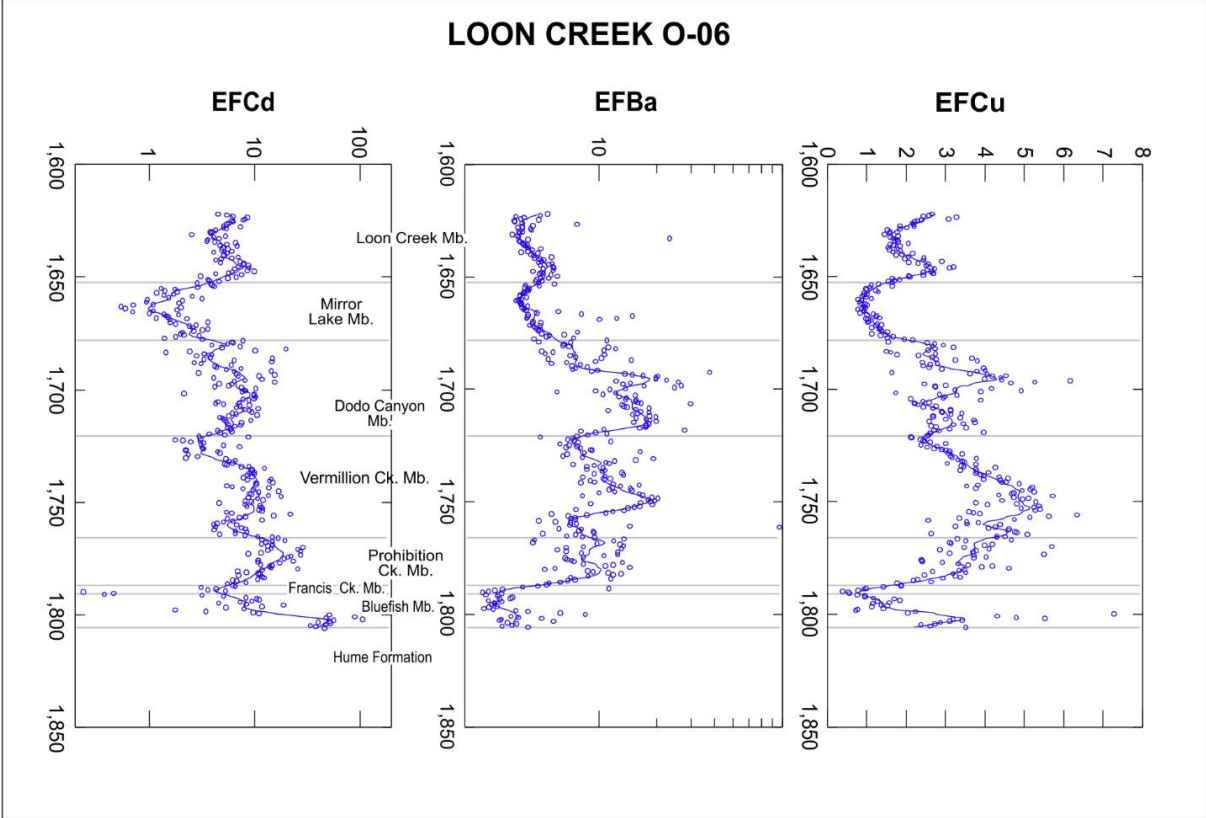


**Figure A1-4.** Loon Creek O-06. Logs of EFCd, EFBa, and EFCu. Solid lines are LOWESS regression with  $\alpha$ -tension 4%. Y axis is measured depth, m.

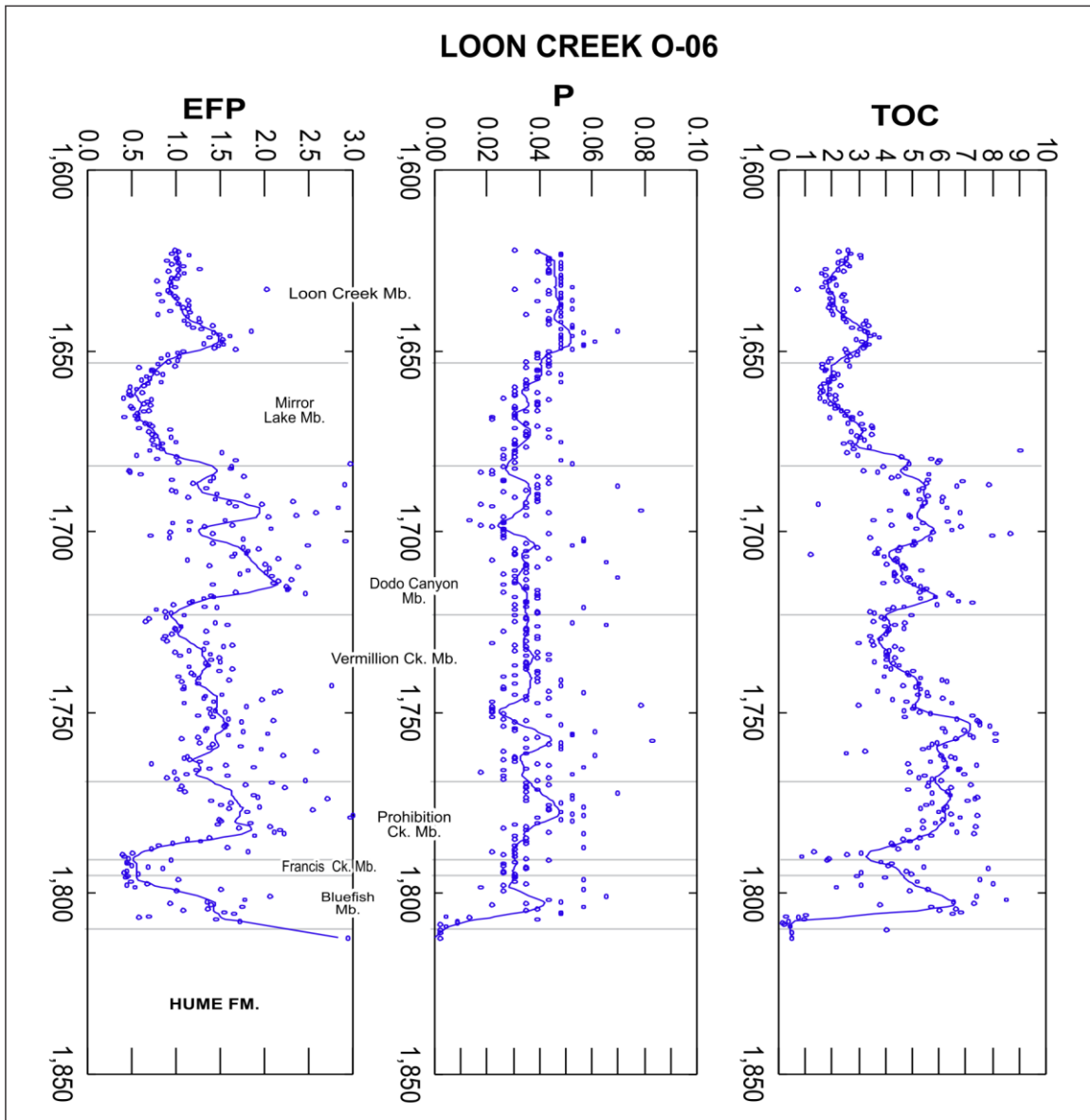


**Figure A1-5.** Loon Creek O-06. Supplementary scatterplots to Fig. 6 of the main text. Solid lines are LOWESS regression with  $\alpha$ -tension 4%. X axis is data cut off at 95% variance. Y axis is measured depth, m.

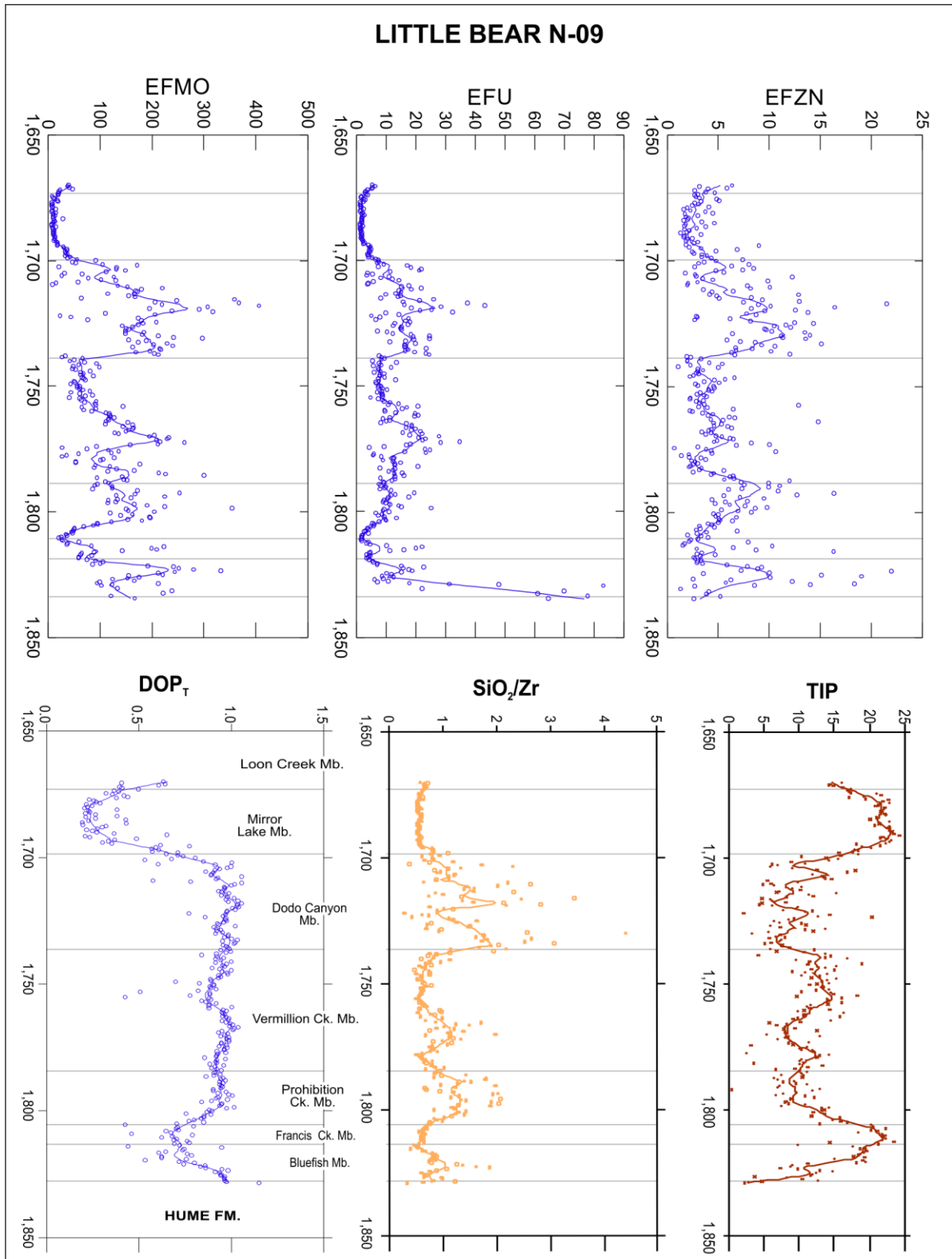


**Figure A1-6.** Little Bear N-09. Supplementary scatterplots to Fig. 3 of the main text and log of EFZn. Solid lines are LOWESS regression with  $\alpha$ -tension 4%. Y axis is measured depth, m.

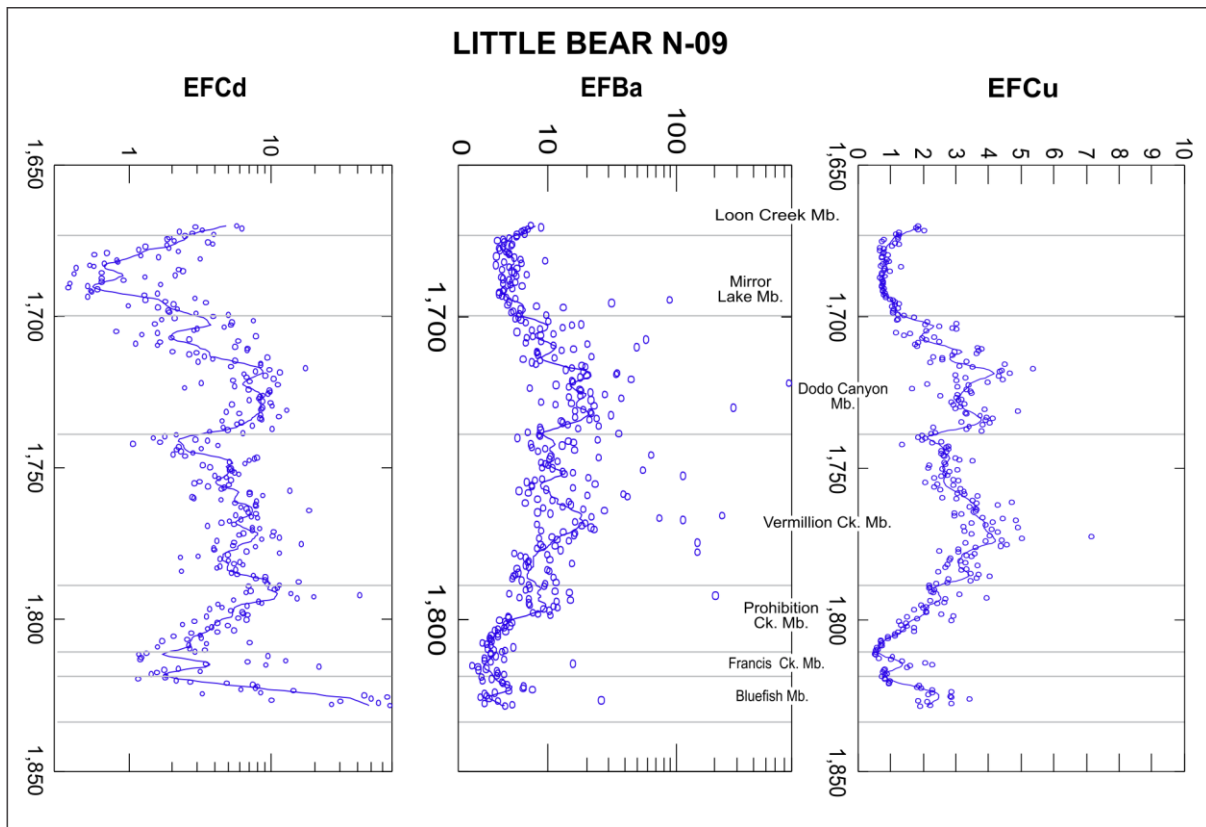


**Figure A1-4.** Little Bear N-09. Logs of EFCd, EFBa, and EFCu. Solid lines are LOWESS regression with  $\alpha$ -tension 4%. Y axis is measured depth, m.

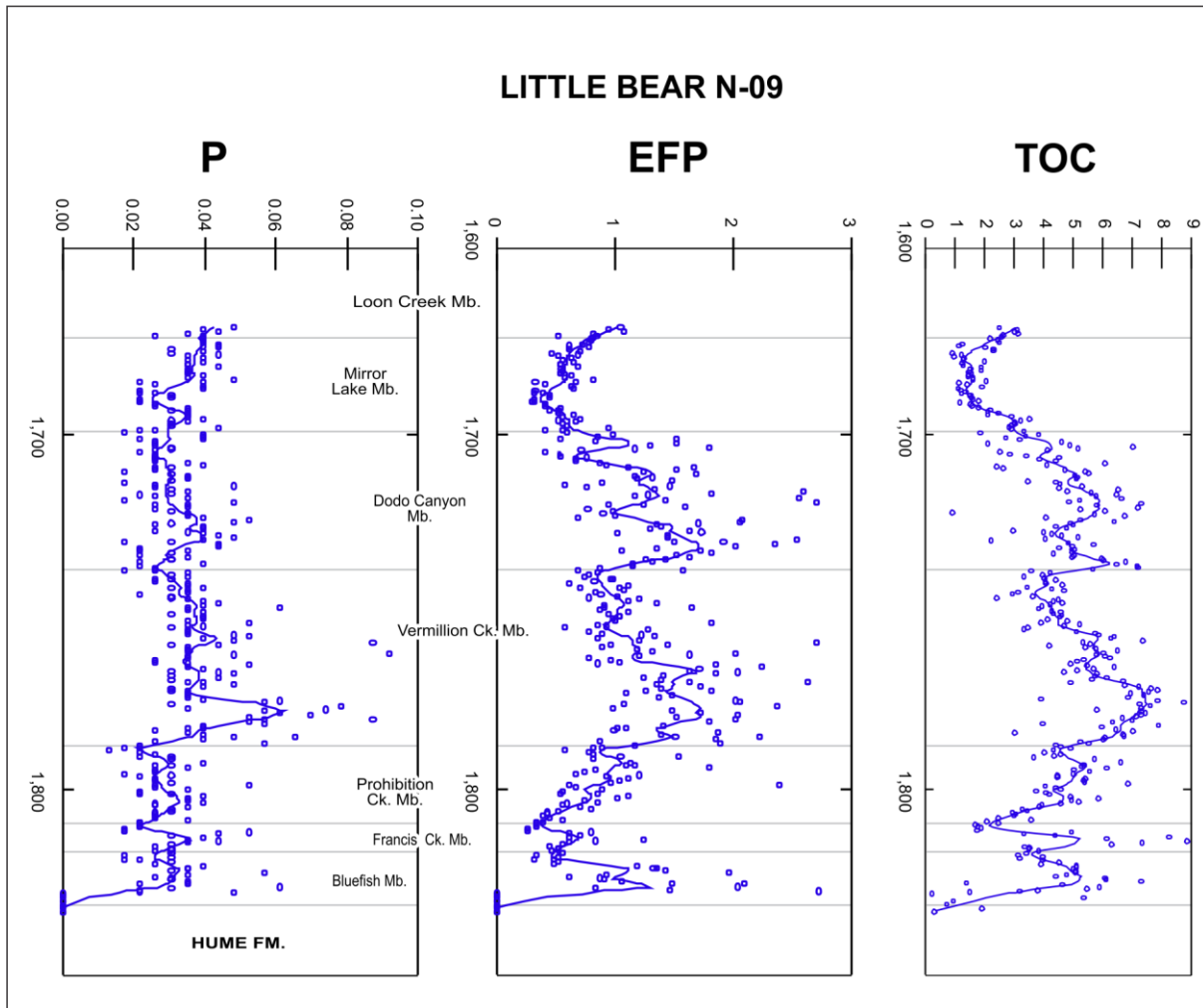


**Figure A1-8.** Little Bear N-09. Supplementary scatterplots to Fig. 6 of the main text. Solid lines are LOWESS regression with  $\alpha$ -tension 4%. X axis is data cut off at 95% variance. Y axis is measured depth, m.

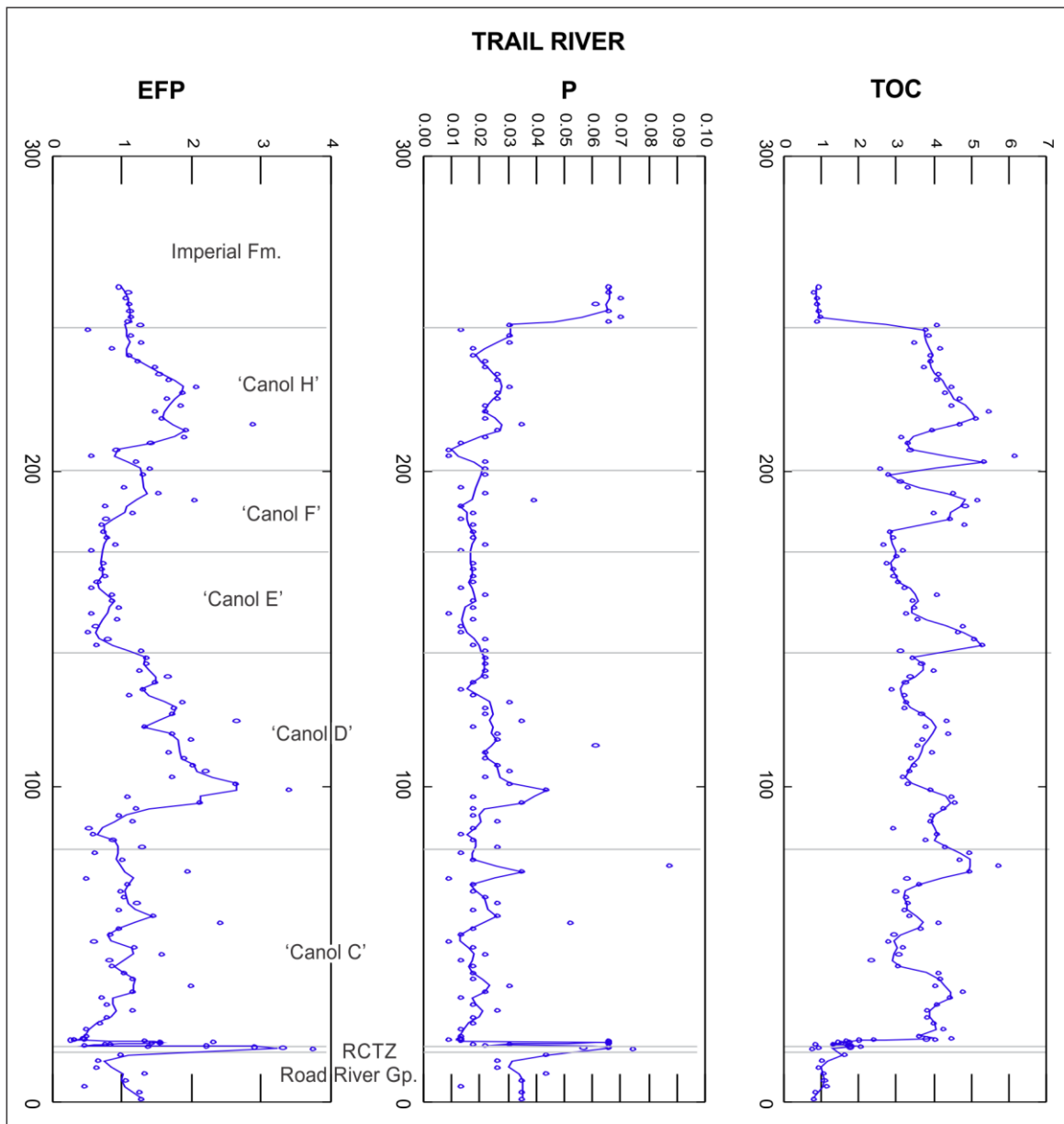


**Figure A1-9.** Trail River section. Supplementary scatterplots to Fig. 6 of the main text. Solid lines are LOWESS regression with  $\alpha$ -tension 4%. X axis is data cut off at 95% variance. Y axis is measured depth, m.

### *Rock-Eval 6 pyrolysis*

TOC values used in this study are reported from pyrolysis-combustion tests conducted at the Organic Petrology and Geochemistry Laboratory in GSC (Calgary) using the Rock-Eval 6 instrument. Approximately 1g of the unwashed core sample was crushed to powder form using a mortar and pestle. A 70 mg aliquot of the sample was then inserted into a stainless steel crucible and heated in an open pyrolysis system. Initially, the samples are heated at 300°C for 3 minutes to volatilize any free hydrocarbons (HC), which are represented by the S1 peak on the pyrograms. The S1 value (mg HC/g of rock) corresponds to the amount of free and adsorbed hydrocarbons generated naturally over time in the rock (Behar et al., 2001).

The next step in the procedure is to heat the samples from 300 to 650°C at a rate of 25°C/minute, which yields the S2 peak. The S2 value (mg HC/g of rock) represents the amount of hydrocarbon released due to thermal cracking of kerogen present in the sample. This is the remaining potential of the sample to generate hydrocarbons if conditions had allowed it. It is important to note that drilling mud contamination and hydrocarbon migration can affect both the S1 and S2 values (Issler et al., 2012), however, in collected core samples the possibility of drilling mud contamination is considered negligible because of pre-sampling surface cleaning and extremely low permeability of shales precluding mud cake formation.

The S3 peak is a measure of the total amount of CO<sub>2</sub> (mg CO<sub>2</sub>/g of initial rock) generated over the entire pyrolysis measurement. The S3 curve accounts for the CO<sub>2</sub> measured during the first stage (0-300°C) and second stage (from 300 to 400 °C), which corresponds to CO<sub>2</sub> generated from organic matter. The S3' curve accounts for the CO<sub>2</sub> generated between 400°C and 650°C, which corresponds to mineral decomposition. The S3 peak is the combination of S3 and S3' (Behar et al., 2001).

The final step is the oxidation of the samples, which measures the total amount of organic carbon generated during this stage. Here, the samples are heated from 300°C to 850°C and the CO and CO<sub>2</sub> are detected by IR cells, producing the S4 curve which measures the residual organic carbon (RC). The S5 curve corresponds to the mineral carbon from CO and CO<sub>2</sub> generated during mineral oxidation (Behar et al., 2001), mainly calcination of carbonate salts.

The sum of the pyrolysable organic carbon (PC) and residual organic carbon (RC) is the total organic carbon (TOC; wt%) in the sample. Tmax is measured at the maximum of the S2 peak and indicates the maturity of the samples, which is dependent on the kerogen type (Tissot et al., 1980). Other calculated parameters include: HI (S2\*100/TOC), OI (S3\*100/TOC) and PI (S1/S2+S3). These parameters aid in identifying the kerogen type (I-IV) and whether the organic matter in the sample is oil vs gas prone.

### ***Access to GSC Paleontological Reports***

Paleontological reports of Geological Survey of Canada / Natural Resources Canada (PaleoReports) are “Protected A” information. These records provide information about the paleontological resources of Canada. Several provinces and territories have issued concerns that bulk public release of fossil site locality data will result in extensive collection, exploitation, or even destruction of sites. This concern varies with jurisdiction. Pre-publication biostratigraphic information delivered in a PaleoReport is considered a transitory result that is subject to changes/updates by the author before the verified version of fossil lists are published. Reference to, or reproduction of, paleontological data and age determinations in publications must be approved by the author of the Paleontological Report. If the author is not available, the Chief Paleontologist, Geological Survey of Canada (Calgary), should be consulted for possible revision. In the present publication, these clauses pertain to citation items (Gouwy, 2016a,b, 2017a,b, 2018).

Questions about PaleoReports shall be directed to the Chief Paleontologist of the Geological Survey of Canada:

Jennifer Galloway, PhD

Research Scientist

Section Head, Paleontology and Collections

Chief Paleontologist

[Geological Survey of Canada \(GSC\), Natural Resources Canada \(NRCan\)](#)

3303 - 33 Street N.W. Calgary, AB, T2L 2A7, Canada  
Tel. +1-587-892-2892  
Fax +1-403-292-4961  
[jennifer.galloway@canada.ca](mailto:jennifer.galloway@canada.ca)

## References

- Behar, F., Beaumont, V. & de Penteadó, H.L. B. 2001. Rock-Eval 6 Technology: Performances and Developments. *Oil and Gas Science and Technology –Rev. IFP*, **56**, 111-134.
- Cleveland, W.S., 1979. Robust locally weighted regression and smoothing scatterplots *Journal of the American Statistical Association*, **74**, 829–836.
- Cleveland, W.S. & Devlin, S.J., 1988. Locally weighted regression: an approach to regression analysis by local fitting. *Journal of the American Statistical Association*, **83**, 596–610.
- Ellis, D.V., & Singer, J.M. 2008. *Well logging for earth scientists*. 2nd ed., Springer Netherlands.
- Fraser, T.A. & Hutchison, M.P. 2017. Litho-geochemical characterization of the Middle–Upper Devonian Road River Group and Canol and Imperial formations on Trail River, east Richardson Mountains, Yukon: age constraints and a depositional model for fine-grained strata in the Lower Paleozoic Richardson trough; *Canadian Journal of Earth Sciences* **54**: 731–765.
- Gal, L.P. & Pyle, L.J., 2012. Petroleum potential data (conventional and unconventional) for Horn River Group from 26 exploration wells - NTS 95N, 96C, 96D, 96E, and 106H, Northwest Territories, Northwest Territories Geoscience Office; N.W.T. Open File Report **2012-009**, 41 p.
- Gouwy, S. 2016a. Reassessment of one Devonian conodont sample from the Bell Creek Member (Hare Indian Formation), Dodo Canyon, NWT collected by Adrienne Jones (NTGO) and submitted under R.B. MacNaughton's MacKenzie Delta and Corridor: Mapping for energy (MATADOR) project in 2011. NTS 096E/03. CON. No. 1767-6. *Geological Survey of Canada, Paleontological Report*, **1-SAG-2016**, 9 p.
- Gouwy, S. 2016b. Report on 15 conodont samples from the Horn River Group (Hare Indian and Canol formations), Prohibition Creek, NWT, NTS 96E/01 collected and submitted by Pavel Kabanov (GEM Shield to Selwyn Basin) Con. No. 1808. *Geological Survey of Canada, Paleontological Report*, **3-SAG-2016**, 15p.
- Gouwy, S. 2017a. Report on nine Devonian conodont samples from the Hume and Hare Indian formations, Rumbly Creek Tributary, NWT, NTS 106G collected by Sofie Gouwy and Pavel Kabanov and submitted under R.B. MacNaughton's Northern Mackenzie Mountains bedrock mapping and stratigraphic studies project (GEM2 Shield-to-Selwyn) Con No 1813-14 to 1813-22. *Geological Survey of Canada, Paleontological Report*, **1-SAG-2017**, 11p.
- Gouwy, S. 2017b. Report on 20 conodont samples from the Bear Rock, Landry, Hume and Canol formations from Powell Creek, Mackenzie Mountains (NWT) NTS 106H collected by Pavel Kabanov and Sofie Gouwy and submitted by Pavel Kabanov (Con No. 1810- 1 to 1810-8 and 1810-17) and under R.B. MacNaughton's Northern Mackenzie Mountains bedrock mapping and stratigraphic studies project (GEM2 Shield-to-Selwyn) (Con No. 1813-1 to 1813-11). *Geological Survey of Canada, Paleontological Report*, **3-SAG-2017**, 17p.
- Gouwy, S.A. 2018. Report on thirteen conodont samples from the Hume and Hare Indian formations from Powell Creek Tributary, northern Mackenzie Mountains (NWT) NTS 106H collected by Pavel Kabanov and Sofie Gouwy and submitted by Pavel Kabanov (Con No. 1810-19 to 1810-29) and under R.B. MacNaughton's northern Mackenzie Mountains bedrock mapping and stratigraphic studies project (GEM2 Shield-to-Selwyn) (Con No. 1813-12 and 1813-13). *Geological Survey of Canada, Paleontological Report*, **3-SAG-2018**, 14p.

- Hutchison, M.P. & Fraser, T.A., 2015. Palaeoenvironment, palaeohydrography and chemostratigraphic zonation of the Canol Formation, Richardson Mountains, north Yukon, in: K. E. MacFarlane and M. G. Nordling (eds.): *Yukon Exploration and Geology 2014*, Yukon Geological Survey, p. 73-98.
- Issler, D.R., Obermajer, M., Reyes, J. & Li, M., 2012. Integrated analysis of vitrinite reflectance, Rock-Eval 6, gas chromatography, and gas chromatography-mass spectrometry data for the Mallik A-06, Parsons N-10 and Kugaluk N-02 wells, Beaufort-Mackenzie Basin, northern Canada; *Geological Survey of Canada, Open File 6978*, 78 p.
- Jacoby, W.G. 2000. Loess: a nonparametric, graphical tool for depicting relationships between variables. *Electoral Studies 19*, 577–613
- Kabanov, P., 2015. Geological and geochemical data from Mackenzie Region. Part I. Devonian cored sections and new geochemical,  $\delta^{13}\text{C}$ -  $\delta^{18}\text{C}$ , and pyrolysis data; *Geological Survey of Canada, Open File 7840*.
- Kabanov, P., 2017, Geological and geochemical data from Mackenzie Corridor. Part VII: new geochemical, Rock-Eval 6, and field data from the Ramparts and Canol formations of northern Mackenzie Valley, Northwest Territories; *Geological Survey of Canada, Open File 8341*, 19 p.
- Kabanov, P., Saad, S., Weleschuk, D.J., & Sanei, H., 2015. Geological and geochemical data from Mackenzie Region. Part II: Lithochemistry and Rock-Eval™ data for the Devonian black shale cored interval of Little Bear N-09 well (Mackenzie Plain, Horn River Group); *Geological Survey of Canada, Open File, 7948*, 23 p.
- Kabanov, P., Gouwy, S., Lawrence, P.W., Weleschuk, D.J., & Chan, W.C. 2016a. Geological and geochemical data from Mackenzie Corridor. Part III: New data on lithofacies, micropaleontology, lithochemistry, and Rock-Eval pyrolysis, Devonian Horn River Group of Mackenzie Plain and Norman Range; *Geological Survey of Canada, Open File 7951*.
- Kabanov, P., Gouwy, S.A. & Chan, W.C., 2016c. Geological and geochemical data from Mackenzie Corridor. Part VI: Descriptions and SGR logs of Devonian outcrop sections, Mackenzie Mountains, Northwest Territories, NTS 106G and 106H, *Geological Survey of Canada, Open File 8173*
- Myers K.J., & Wignall P.B. 1987 Understanding Jurassic organic-rich mudrocks – New concepts using gamma-ray spectrometry and paleoecology: Examples from the Kimmeridge Clay of Dorset and the Jet Rock of Dorshire. In: Legget, J.K. & Zuffa, G.G. (eds) *Marine Clastic Sedimentology*; Graham and Trotman, 172-189.
- Pyle, L.J., Gal, L.P., & Lemiski, R.T., 2011. Measured sections and petroleum potential data (conventional and unconventional) of Horn River Group outcrops – Part 1, NTS 96D, 96E, and 106H, Northwest Territories. *N.W.T. Open File Report 2011-09*, 116 p.
- Pyle, L.J. & Gal, L.P., 2012. Measured sections and petroleum potential data (conventional and unconventional) of Horn River Group outcrops, NTS 95M, 95N, 96C, 96D, 96E, 106H, and 106I, Northwest Territories – Part II. *Northwest Territories Geoscience Office, N.W.T. Open File Report 2012-008*, 114 p.
- Pyle, L.J. & Gal, L.P., 2013. Measured sections and petroleum potential data (conventional and unconventional) of Horn River Group outcrops, NTS 96C, 96E, and 106H, Northwest Territories – Part III; *Northwest Territories Geoscience Office, N.W.T. Open Report, 2013-005*, 73 p.
- Pyle, L.J., Gal, L.P., & Fiess, K.M., 2014. Devonian Horn River Group: A Reference Section, Lithochemical Characterization, Correlation of Measured Sections and Wells, and Petroleum-Potential Data, Mackenzie Plain area (NTS 95M, 95N, 96C, 96D, 96E, 106H, and 106I), NWT. *Northwest Territories Geoscience Office, NWT Open File, 2014-06*, 70 p.
- Tribovillard, N., Algeo, T., Lyons, T.W., & Riboulleau, A. 2006. Trace metals as paleoredox and paleoproductivity proxies: an update. *Chemical Geology, 232*, 12–32.